

Superconducting Transition Temperature, Lattice Instability, and Electron-to-Atom Ratio in Transition-Metal Binary Solid Solutions*

E. W. Collings, J. C. Ho,[†] and R. I. Jaffee

Battelle, Columbus Laboratories, Columbus, Ohio 43201

(Received 19 April 1971; revised manuscript received 15 November 1971)

In a series of transition-metal binary alloys, as the average electron-to-atom ratio \bar{z} decreases from 6.0 to 4.0, the measured electronic-specific-heat coefficient γ , and with it the average Fermi density of states $n(E_F)$ rises to a maximum near $\bar{z}=4.4$. From an analysis of the coupled results of low-temperature calorimetric and magnetic susceptibility measurements it has been shown in a previous paper that, at least for the Ti-Mo system, the maximum in average $n(E_F)$ was induced through the influence of submicroscopic metallurgical inhomogeneities (clustering and second-phase precipitation) present in the as-quenched $\bar{z} \lesssim 4.3$ material, and was not a property of the (hypothetical) single-phase bcc alloy. In addition, it was demonstrated that were it not for this precipitation, the effects of which became increasingly noticeable as \bar{z} decreased below about 4.3, $n(E_F)$ would otherwise increase monotonically as \bar{z} decreased from 6.0 to 4.0. In this paper, which is an extension of that work, the superconducting behavior of Ti-Mo is explored. The results of calorimetric measurements yield both a superconducting transition temperature T_c and a Debye temperature Θ_D which (through the elastic constants c_{ij}) may be related to lattice stability. Again, if we postulate the existence of single-phase bcc Ti-Mo alloys, in which precipitation for $\bar{z} \lesssim 4.3$ has been inhibited, a semiquantitative argument shows that T_c should also increase monotonically with decreasing \bar{z} . As a generalization of this result, it is suggested that in the well-known double-humped curve of T_c vs \bar{z} for transition-metal binary alloys the local maximum near $\bar{z}=4.4$ is induced (or at least strongly contributed to) by microstructural effects, rather than being a property of single-phase bcc alloys. Finally, a connection is made between the superconducting behaviors of transition-metal binary alloys, which might be regarded as low-perturbation systems, and the tightly bound transition-metal-nontransition-metal intermetallic compounds, for which the very opposite is true. The coupling parameter is "lattice stability" which decreases with decreasing \bar{z} , in the range under consideration, for both the alloys as well as the compounds. The increase of T_c with decreasing \bar{z} generally terminates at the edge of the regime of phase stability (e.g., at the low-concentration limit of the equilibrium single-phase bcc field, in the case of Ti-Mo alloys).

I. INTRODUCTION

We offer the following discussion of relationships among superconducting transition temperature (T_c), Debye temperature (Θ_D), electron-to-atom ratio (\bar{z}), and phase stability of transition-metal binary (T_1 - T_2) alloys, to complement some published studies by the Bell Lab¹ and Orsay² groups on superconductivity and lattice stability in the β -W intermetallic compounds. A connection between these two classes of materials with regard to superconductivity has already been made by Matthias,^{3,4} whose remarkable T_c -vs- \bar{z} rule embraces indiscriminately both low-perturbation alloys and tightly bound intermetallic compounds.

For several years we have been examining the superconductive, microstructural, electronic, and mechanical properties of the Ti-Mo alloy system as a representative of the set of "near-adjacent" transition-metal binary alloys in the electron-to-atom ratio range 4-6, based on group-IV transition elements. Included in such a set of alloys (designated Ti- T_2 , Zr- T_2 , etc.) are the technically

important superconductors Ti-Nb and Zr-Nb. We emphasize at the outset that the metallurgical and superconducting behaviors of all such alloys cannot be represented *completely* by any single system, but that they do possess some important common characteristics which can be usefully discussed with reference to the properties of a prototype system, such as Ti-Mo, which we have studied in great detail.

At sufficiently high temperatures Ti-Mo alloys are all single-phase bcc (β). In equilibrium at, say, 300 °C a two-phase [hcp(α) + β] structure occupies most of the \bar{z} range 4 to about 4.4; but on quenching those alloys from the β field to room temperature, a sequence of nonequilibrium structures appears. This behavior is summarized in Fig. 1. The ω -phase referred to in Fig. 1(c) is a precipitate, hexagonal in crystal symmetry, which in the as-quenched alloys is submicroscopic in size (~ 100 Å diam) and which occurs with increasing density as the solute concentration decreases toward the M_s line. The phase transformations of course express the instability of the

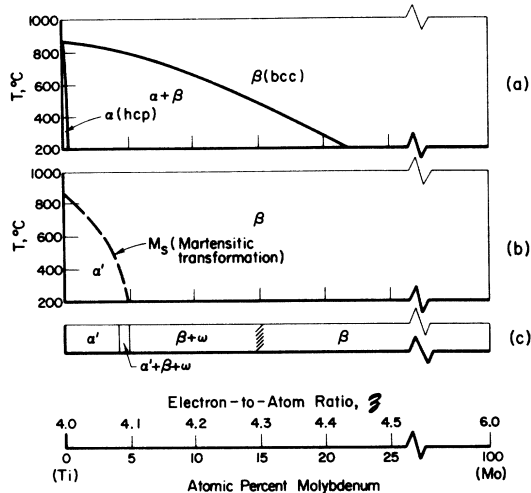


FIG. 1. (a) Portion of the Ti-Mo equilibrium phase diagram. (b) Representation of the structures present in Ti-Mo alloys after quenching from, say, 1000 °C to the temperatures indicated. The martensitic structure (α') forms spontaneously on quenching. The occurrence of ω phase has some time dependence and cannot be adequately represented on such a diagram. (c) Structures observed, or deduced, to be present in 30-g ingots after quenching into iced brine. The upper concentration limit of ω phase is somewhat uncertain since there is in fact no sharp upper boundary to the ($\beta + \omega$) regime of structural fluctuations.

β structure ($\bar{z}_{\text{Ti-Mo}} \lesssim 4.3$) at room temperature and below; however, in a discussion of lattice stability and related effects it is important to be able to estimate the properties of *single-phase* β alloys ($\bar{z} \lesssim 4.3$) for comparison with those in the quenched, and even in the equilibrium states. This we do with the aid of various extrapolation procedures, some of which are terminated at M_s , since at about that point one of the extrapolated elastic shear moduli [viz, $\frac{1}{2}(c_{11} - c_{12})$] vanishes. We will refer to single-phase β -Ti-Mo alloys, at room temperature, in the composition range 0–15-at. % Mo as “*unstable*.” They will be divided into two classes: those below the M_s composition ($4\frac{1}{2}$ -at. % Mo) will be referred to as “*absolutely unstable*,” since for these the extrapolated elastic constants yield $c_{11} < c_{12}$, while those in the range $5 < \text{at. \% Mo} < 15$, which, although normally unstable, do not yield unphysical elastic moduli, will be designated “*virtual*” β -Ti-Mo.

The numerous investigations of the low-temperature calorimetric properties of transition-metal binary alloys, including the Ti- T_2 etc., systems, have been comprehensively reviewed by Heiniger, Bucher, and Muller.⁵ Characteristic of all curves of electronic-specific-heat coefficient (γ) vs \bar{z} for such alloys is a pronounced local maximum occurring near $\bar{z} = 4.4$. Based on magnetic and calorim-

etric studies of the Ti-Mo system,^{6,7} we assert that this maximum is induced, at least in part, by the presence of ω phase which occurs in the as-cast or as-quenched alloys within the concentration range for which $\bar{z} \lesssim 4.3$. The measured γ is an average of γ_β and the much smaller quantity γ_ω . We have also argued⁷ that were the alloy to persist in its single-phase β form, then γ , and with it the Fermi density of states $n(E_F)$, would continue to increase monotonically as \bar{z} decreased below about 4.3. In this paper, we commence with an outline of the empirical procedure used to perform this extrapolation of γ and $n(E_F)$ for virtual β -Ti-Mo, and go on to show how the technique can be extended to include T_c and the low-temperature calorimetric Debye temperature Θ_D . We conclude by discussing the results in terms of the relationships between T_c , Θ_D , and lattice structure and stability, with \bar{z} as a parameter.

II. EXPERIMENTAL DETAILS

A. Specimen Materials

Ti-Mo specimens, herein designated TM-1 to TM-70 (where the numbers refer to the nominal Mo concentrations in atomic percent) were cut from well-homogenized arc-melted ingots prepared from high-purity starting materials.⁸ The chemically analyzed Mo concentrations are listed in Table III. To obtain reproducible microstructures, the alloys were all annealed at 1300 °C for 8 h in a Ti-gettered-argon environment, and quenched into iced brine. The specific-heat specimens weighed about 30 g, while those for the magnetic susceptibility measurements were typically 200 mg. Small pieces were also removed for optical and electron microscopy.

B. Experimental Techniques

As in two of the authors' previously described studies of the Ti-Mo system,^{6,7,9-11} the principal experimental technique used was low-temperature calorimetry, which yields not only γ and a low-temperature Θ_D , but, under favorable conditions, a superconducting transition temperature T_c . The three quantities γ , Θ_D , and T_c so obtained are all interrelated. In addition, from the relative height of the specific-heat jump $[\Delta(C/T)/\gamma]$ at T_c it is possible to derive an estimate of the fraction of the sample which goes superconducting at about that temperature. It is important to note that in the quenched two-phase ($\beta + \omega$)-Ti-Mo alloys, the superconducting transition was bulk.⁶ This property of ($\beta + \omega$)-phase alloys, which owes its origin to superconductive proximity effects, is to be discussed in a subsequent paper.

Magnetic susceptibility was measured by the Curie technique with reference to a specimen of

TABLE I. List of approximate relationships used in the derivation of T_c/Θ_D for virtual β -Ti-Mo alloys.^a

T_c and Θ_D	
$\ln(T_c/\Theta_D)$	$= \text{const} - (1/V)n(E_F)^{-1}$ (1) ^b
$n(E_F)$	$= 0.212\gamma^0$ (2)
γ^0	$= \gamma/(1+\lambda)$ (3)
V_{app}	$= V/(1+\lambda)$ (4)
$\ln(T_c/\Theta_D)$	$= \text{const} - (1/V_{\text{app}})(0.212\gamma)^{-1}$ (5)
Evaluation of λ	
λ	$= n(E_F)V$ (6) ^c
	$= 0.212\gamma V_{\text{app}}$ [using (2)-(4)]
V_{app}	$= 0.26$ (experimental value from Fig. 2)
λ	$= 0.0551\gamma$ (7)
χ, χ	
χ^0	$= 4.72n(E_F)$ (8)
χ_{spin}	$= 64.7n(E_F)$ (9) ^d
	$= 13.71\gamma^0$ (8)
χ	$= \chi_{\text{spin}} + \chi_{\text{orb}}$ (9) ^d
γ	$= \gamma^0/(1 - 0.551\gamma^0)$ [using (3) and (7)] (10)

^aSee also E. W. Collings and J. C. Ho, Phys. Status Solidi **43**, K123 (1971).

^bAfter J. Bardeen, L. N. Cooper, and J. R. Schrieffer, Phys. Rev. **108**, 1175 (1957); and P. Morel, J. Phys. Chem. Solids **10**, 277 (1959).

^cSee, for example, A. M. Clogston *et al.*, Phys. Rev. Letters **9**, 262 (1962).

^dThese are the dominant susceptibility components. For a full discussion of susceptibility components of some transition metals, see E. W. Collings and J. C. Ho, Phys. Rev. B **4**, 349 (1971).

high-purity Pt whose susceptibility (0.977 $\mu\text{emu/g}$ at 293 K) and susceptibility temperature dependence (6.3×10^{-10} emu/g K within 260–300 K) have been given by Budworth *et al.*¹² Measurements were made both at room temperature and, as functions of temperature in the high-temperature β regime, up to about 1400 K.

III. RESULTS AND ANALYSIS

The primary aim of the experiment was to derive an estimate of the δ dependence of T_c for virtual β -Ti-Mo alloys. The required T_c values were deduced from a semilog plot of T_c/Θ_D vs $(0.212\gamma)^{-1}$ after having first obtained a set of γ values for

virtual β -Ti-Mo. These were acquired in a manner described in detail elsewhere⁷ and outlined in Sec. III C. The procedure used was to combine the results of low-temperature calorimetry [$\gamma \rightarrow n(E_F)$] and room-temperature magnetic susceptibility [$(\chi_{\text{spin}} \rightarrow n(E_F))$] for quenched Ti-Mo (≥ 20 -at. % Mo; equilibrium β) alloys, with extrapolated room-temperature magnetic-susceptibility data for virtual β -Ti-Mo ($\delta \lesssim 4.3$) deduced from experiments performed in the elevated-temperature equilibrium- β field (Fig. 1).

A. Formulas and Approximations

The expressions used in analyzing the experimental data are listed in Table I, the quantities and units employed therein being defined in Table II. A Bardeen-Cooper-Schrieffer (BCS)¹³ expression, as modified by Morel,¹⁴ is employed to relate T_c to the other experimental quantities. Our justifications for using the BCS-Morel equation are as follows: (i) It is directly applicable to the calorimetrically measured quantities. (ii) In Ti-Mo the superconductive electron-phonon coupling, although not weak, is certainly not strong. (iii) It is felt that the level of approximation involved in using such a model to describe the superconductivity is consistent with that existing elsewhere in the analysis, viz., in the use of the conventional free-electron expressions to relate χ_{spin} and γ^0 to $n(E_F)$, and hence to each other. And (iv) the goal of the experiment is not to derive exact numbers for T_c but rather to obtain a semiquantitative estimate of T_c as a function of decreasing δ in virtual β -Ti-Mo, for comparison with the behaviors of other properties, and other materials, in the same δ range.

B. Relationship between T_c/Θ_D and γ

The modified BCS-Morel relationship between the calorimetrically derived quantities T_c , Θ_D , and γ [Table I, Eq. (5)] shows that a semilog plot of T_c/Θ_D vs $(0.212\gamma)^{-1}$ will be linear for a series of alloys if $V_{\text{app}} = \text{const}$. Figure 2, constructed from rows 4–6 of Table III, demonstrates that the rele-

TABLE II. Definitions of symbols and units employed in Table I.

Symbol	Quantity	Units employed
χ	Measured magnetic susceptibility	$\mu\text{emu/mole}$
χ_{orb}	Orbital paramagnetic susceptibility	$\mu\text{emu/mole}$
χ_{spin}	Pauli spin paramagnetism	$\mu\text{emu/mole}$
γ	Measured electronic-specific-heat coefficient	mJ/mole deg^2
γ^0	Above, after correction for many-body effects	mJ/mole deg^2
$n(E_F)$	Fermi density of states for one spin direction	(states)/eV (atom)
Θ_D	Debye temperature	K
T_c	Superconducting transition temperature	K
λ	Electron-phonon coupling constant	number
V	Electron-(phonon)-electron pairing potential	eV (atom)

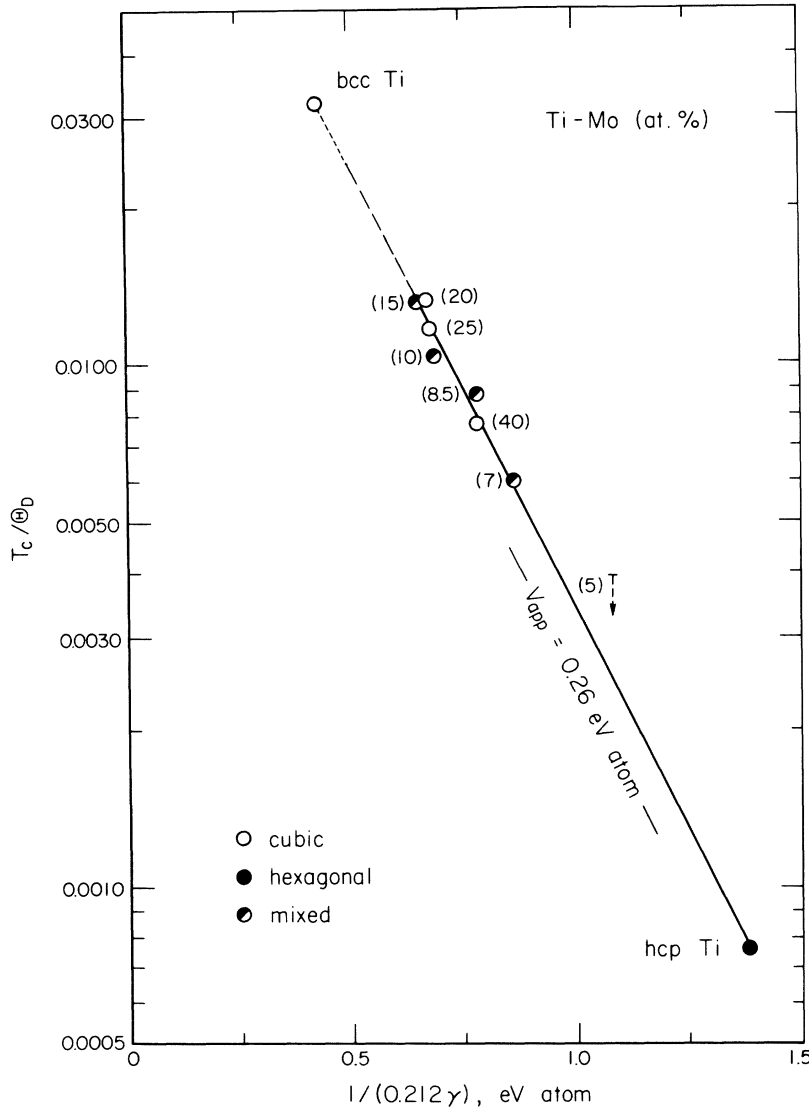


FIG. 2. Semilog plot of T_c/Θ_D vs $(0.212\gamma)^{-1}$ based on the BCS-Morel expression $T_c/\Theta_D \propto e^{-1/n(E_F)V}$. The straight line, whose slope is $(-0.26 \text{ eV atom})^{-1}$ has been extrapolated into the "virtual" (dashed line) and "absolutely unstable" (chain line) regimes. The bcc-Ti point, based on the experimentally estimated γ value is indicated.

vant data for TM-7 through TM-40, together with that for hcp(α) Ti, do indeed lie close to a straight line whose slope yields $V_{app} = 0.26 \text{ eV atom}$. Figure 3, an enlargement of the low-concentration end of Fig. 2, indicates that by a short extrapolation, values of T_c/Θ_D for virtual β -Ti-Mo are available, provided that the corresponding γ values can first be obtained.

C. Extrapolation of the $n(E_F)$ -Related Quantities

A full description of the procedure used to extrapolate γ into the virtual β -Ti-Mo regime has appeared in the proceedings of the Electronic Density of States Symposium,⁷ so that only a brief outline of the method used will be given here. The consecutive steps taken in the data analysis for γ are described by Table III. Recognizing that the slope of the BCS-Morel plot (Figs. 2 and 3) provides suf-

ficient information to correct for many-body effects over the whole alloy concentration range (as in the second section of Table I) the heart of the extrapolation procedure for γ is the pair of Eqs. (9) and (10) of Table I in the form

$$\chi = \chi(\gamma^0) + \chi_{orb}, \quad (9')$$

where

$$\gamma^0 = \gamma^0(\gamma). \quad (10')$$

From the results of magnetic and calorimetric experiments performed on the quenched alloys TM-20 to TM-100, whose structures are single-phase bcc, Eqs. (9) and (10) are employed to evaluate χ_{orb} , whose¹⁵ estimated composition dependence is presented in Fig. 4. The successive steps taken in this part of the analysis are described by rows 4 and 7-10 of Table III. Using

TABLE III. Analysis of joint low-temperature specific-heat and magnetic-susceptibility data. Measured quantities are enclosed in boxes. The "final result" is the underscored γ (unstable β) data for Ti-Mo (0-15 at. %), row 14.^a

Alloy Designation	Pure Ti	TM-1	TM-2	TM-3	TM-5	TM-7	TM-8-1/2	TM-10	TM-15	TM-20	TM-25	TM-40	TM-70	Pure Mo	Symbol in Figure 5	Comments
Metallurgical Data																
1 Measured at.% Mo	0	0.9 _g	1.9 ₁	2.8 ₇	5.1 ₆	6.9 ₆	8.6 ₆	10.3 ₀	14.9 ₂	19.3 ₈	25.3 ₆	39.8 ₁	71.0 ₂	100		
2 Microstructures of quenched alloys	Thermal martensite (α')		bcc (β) plus α' -phase										bcc (β)			
3 Structural stability of single-phase β alloys	Unstable under quenching to room temperature										Stable at room temperature					
	"Absolutely unstable" Ti-Mo										"Virtual" Ti-Mo					
Low Temperature Specific Heat Data																
4 γ (mJ/mole-deg ²)	3.3 _g	3.9 ₅	4.0 ₅	4.5	4.4	5.5	6.1	6.9	7.3	7.1	7.0	6.1	2.6 ₅	1.8 ₅	▽	Plotted together in Fig. 2 in the format $\log T_c/\Theta_D$ versus $1/(0.212 \gamma)$, yielding $V_{app} = 0.26$ eV/atom for use in transforming γ^{me}, γ^{sp} using $\lambda \cong 0.212 \gamma V_{app}$.
5 T_c (K)				<1.5	2.1	2.8	3.3	3.8 ₅	4.0	3.7	2.8	<1.5			○	
6 Θ_D (K)	420	330	350	380	350	320	320	295	305	320	365	410	470		□	
7 γ^q [quenched β]									5.17	5.05	4.57	2.31	1.68			$\gamma^q \cong \gamma/(1+\lambda)$ Table 1, Equation (3)
Magnetic Susceptibility Data																
8 χ_{spin} [quenched β]																$\chi_{spin} \cong 13.71 \gamma^q$ Table 1, Equation (8)
9 χ_{total}^{300K} (μ emu/mole)	151.8	157.2	158.9	164.3	168.3	187.9	195.8	201.0	204.4	202.8	200.3	190.4	132.2	84.4		Directly measured at room temperature
10 χ_{orb} ["unstable" and quenched β]	(134.4)	(134.3)	(134.2)	(134.1)	(134.0)	(133.9)	(133.6)	(133.5)	(133.0)	132.6	130.8	127.8	100.5	61.4		$\chi_{orb} \cong \chi_{total} - \chi_{spin}$ values extrapolated into the 0-15 at.% region are bracketed
11 χ_{total}^{300K} [unstable β]	231.4	229.0	227.0	225.0	221.0	217.5	214.5	212.2	206.2						◐	By extrapolation of the high-temperature (equilibrium bcc) data, to room temperature. Graphically smoothed
12 χ_{spin} [unstable β]	97.0	94.7	92.8	90.9	87.0	83.6	80.9	78.7	73.2						◑	$\chi_{spin} \cong \chi_{total} - \chi_{orb}$
Final Analysis																
13 γ^q [unstable β]	7.0 _g	6.9 ₁	6.7 ₇	6.6 ₃	6.3 ₅	6.1 ₀	5.9 ₀	5.7 ₄	5.3 ₄							$\gamma^q \cong \chi_{spin}/13.71$
14 γ [unstable β]	11.6 ₀	11.1 ₅	10.8 ₀	10.4 ₅	9.7 ₆	9.1 ₈	8.7 ₄	8.4 ₀	7.5 ₆						▽	$\gamma \cong \gamma^q/(1-0.0551 \gamma^q)$ Table 1, Equation (10)

^aData extrapolated into the " α' " range $0 \leq [\text{Mo}] < 4.5$ at. % must be interpreted with considerable caution.

^bApplying the data of row 14 to this curve yields values of (T_c/Θ_D) for "virtual" bcc Ti-Mo (5-15 at. %) for use in estimating the behaviors of T_c and Θ_D in these alloys.

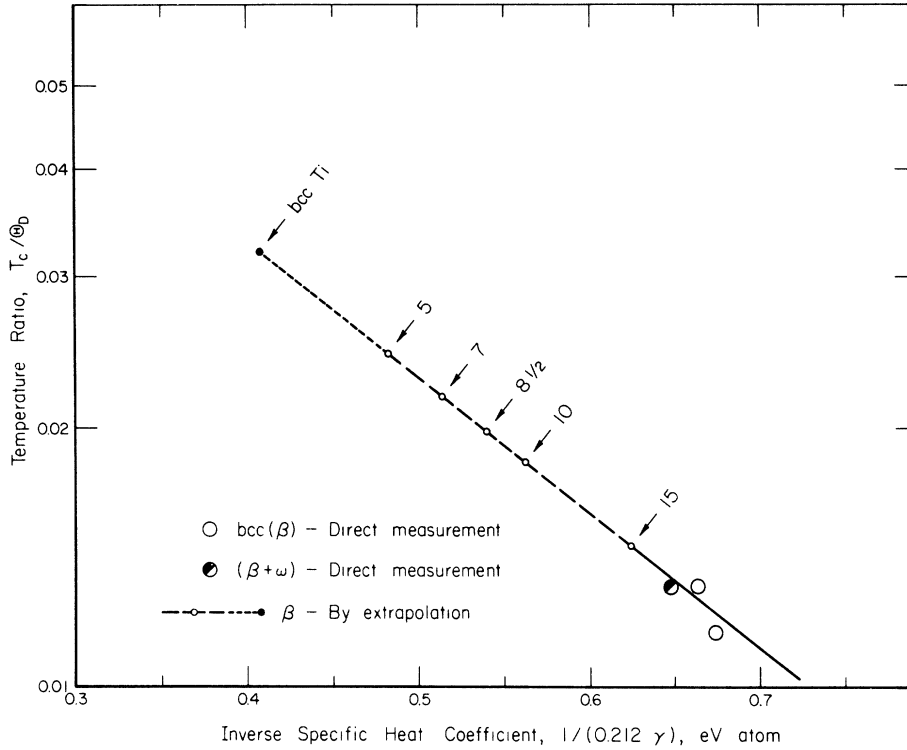


FIG. 3. Extrapolated segment of Fig. 2 shown on an expanded scale. The points correspond to virtual bcc Ti-15 through Ti-5, based on the experimentally derived extrapolated γ values (Table III). The chain line indicates extrapolation into the "absolutely unstable" regime, the properties of which are undefined. Values of the quotient T_c/Θ_D obtained from this graph were used in the assignment of values of the individual quantities T_c and Θ_D for unstable Ti-Mo.

room-temperature-susceptibility values for unstable β -Ti-Mo, obtained by extrapolating back the almost-temperature-independent elevated-tempera-

ture susceptibility data, reapplications of Eqs. (9) and (10) yield the required values of γ for unstable β -Ti-Mo. These steps are delineated in the final

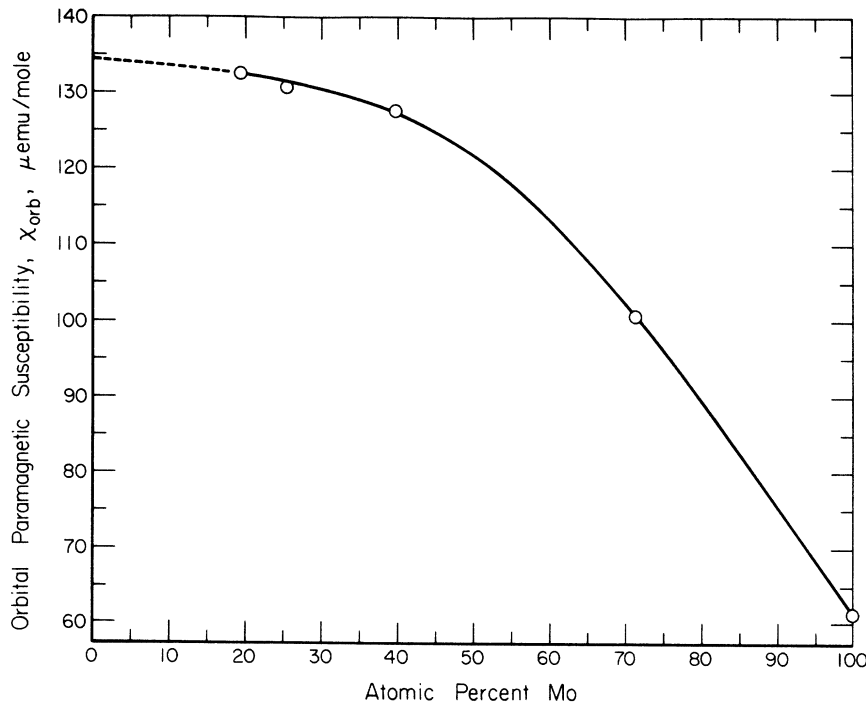


FIG. 4. Plot of orbital paramagnetic susceptibility χ_{orb} vs composition for Ti-Mo alloys. The curve through the data points has been extrapolated into the unstable regime. The intercept yields $\chi_{orb}(Ti_{bcc}) \approx 134 \mu\text{emu/mole}$ (Ref. 15).

TABLE IV. Estimation of T_c/Θ_D for virtual bcc Ti-Mo alloys, and selection of corresponding pairs of values of T_c and Θ_D .

1	2	3	4	5
Alloy designation	Estimated γ for dilute β Ti-Mo from Table III	Corresponding T_c/Θ_D ratio from Fig. 3	Selected Θ_D	T_c from $T_c = (T_c/\Theta_D)\Theta_D$
bcc-Ti ^a	11.60	0.032 ₀	200	6.4
TM-5	9.76	0.024 ₄	207	5.0 ₅
TM-7	9.18	0.021 ₈	220	4.8 ₀
TM-8 $\frac{1}{2}$	8.74	0.019 ₈	232	4.5 ₉
TM-10	8.40	0.018 ₂	243	4.4 ₂
TM-15	7.56	0.014 ₆	281	4.1 ₀

^aData extrapolated into the α' range $0 \leq [\text{Mo}] < 4.5$ at. % must be interpreted with considerable caution, e. g., when calculated from extrapolated c_{ij} values, Θ_D for Ti-Cr is certainly unphysical within $2.7 \leq [\text{Cr}] \leq 4.5$ at. %.

four rows of Table III.

D. Qualitative Behavior of T_c

The γ 's derived in the manner outlined above may be applied to Fig. 3 in order to obtain T_c/Θ_D for virtual β -Ti-Mo alloys. The values so deduced are presented in Table IV, column 3. Note that, with the exception of β -Ti which is listed for reference, alloys within the absolutely unstable regime are not tabulated. The problem which next arises is the estimation of the behavior of T_c itself in the virtual β -Ti-Mo regime, i. e., the extraction of separate sets of values of T_c and Θ_D .

Important data from Table III which are presented in Fig. 5 are (i) directly measured and extrapolated values of γ and χ —curves a and b, respectively, and (ii) the directly measured values of T_c and Θ_D —curves c and d. It is suggested that the scaling exhibited by the directly measured quantities γ , χ , and T_c should also be a characteristic shared by the extrapolated curves. In other words, we suggest that T_c for virtual β -Ti-Mo continues to increase monotonically; and that the local maximum at $\delta \cong 4.3$, observed in the results of the direct measurements (on β and $\beta+\omega$ alloys), is induced by the ω -phase precipitation in the lower-concentration alloys. This conclusion is confirmed by the results of a separate set of experiments on TM-10, in which ω -phase precipitation is incomplete in the as-quenched alloy. By carrying out *directly* what is in principle the converse of the above *extrapolation* procedure we have shown, in a series of "aging" experiments,¹⁶ that T_c continues to decrease as the ω -phase precipitate develops.

As a first step in obtaining semiquantitative estimates of extrapolated T_c , we consider the T_c/Θ_D ratios listed in Table IV, column 3; with the preliminary assumption that the extrapolated Θ_D is constant and equal to the minimal directly measured value (viz., 295 K for TM-15). In this case the locus of extrapolated T_c seems excessively high

(rising to 7.2 K at TM-5). To obtain a more conservative estimate of T_c we should allow for a possible decrease in Θ_D ; behavior which itself could be interpreted as being indicative of a softening of the lattice in the unstable regime. At this stage it is appropriate, both for the present purpose and for future use, to consider in more detail the behavior of Θ_D in unstable β -Ti-Mo and similar alloy systems.

E. Debye Temperature Θ_D in Low-Concentration Ti-T₂ Alloys

Calorimetric measurements of the type described above (e. g., Refs. 7 and 17) are the only sources of information relating to Θ_D in Ti-Mo. Fortunately, however, for a closely related system Ti-Cr, a comprehensive set of elastic-constant data is available through the work of Fisher and Dever,¹⁸ who have measured the elastic constants c_{ij} of that system both at room temperature and as functions of temperature in the elevated-temperature β regime. From such c_{ij} 's, very reliable values of Θ_D are easily calculable by Anderson's method.¹⁹ Moreover, it is also possible to calculate "extrapolated" Θ_D 's for alloys in the unstable regime, by inserting in Anderson's formulas room-temperature values of the c_{ij} 's obtained by extrapolation from the elevated-temperature single-phase field. Thus, the elastic-constant-based analysis serves to complement the low-temperature calorimetric Θ_D data by yielding Θ_D values for structures inaccessible to low-temperature techniques (in much the same way that our magnetic-susceptibility measurements complemented the low-temperature electronic-specific-heat work).

From Fisher and Dever's¹⁸ published data for the elastic constants of five Ti-Cr alloys, plots of the temperature dependences of c_{11} , c_{12} , and c_{44} have been drawn as in Fig. 6(a); also values of Θ_D , calculated by Anderson's method and tabulated in Appendix A (Table VI), are plotted in Fig. 6(c). Using the linearly extrapolated elastic constants of Fig. 5(a), the concentration dependence of Θ_D

in unstable Ti-Cr was explored. The results of the computations, outlined in Appendix B, are shown in Fig. 6(b). Of particular interest is the rapid drop in Θ_D just below the composition for which $c_{11} = c_{12}$ (viz., 5.0₃-at. % Cr, according to Table VII in Appendix B). As discussed in Appendix C this is associated with the threshold of martensitic transformation which occurs between 5- and 6-at. % Cr. At lower solute concentrations than this, i. e., in the absolutely unstable regime, Θ_D for β -Ti-Cr is unphysical.

F. T_c and Θ_D for Ti-Mo

Returning now to Ti-Mo, pairs of values of T_c

and Θ_D are selected, as listed in Table IV, using smoothness as one criterion. That is to say, T_c may be extrapolated into the unstable regime as a smooth continuation of the directly measured stable- β locus [Fig. 5, curve c] provided that, from about $\delta = 4.3$, Θ_D is permitted to drop so as to form a smooth low-lying branch in the manner illustrated in curve d of Fig. 5. The data are re-plotted in Fig. 6(c) alongside that for Ti-Cr in the same δ range. In Appendix C we present arguments to the effect that this pair of curves shows mutual consistency, provided due consideration is given to differences in the microstructural characteristics of the respective alloy systems. Some

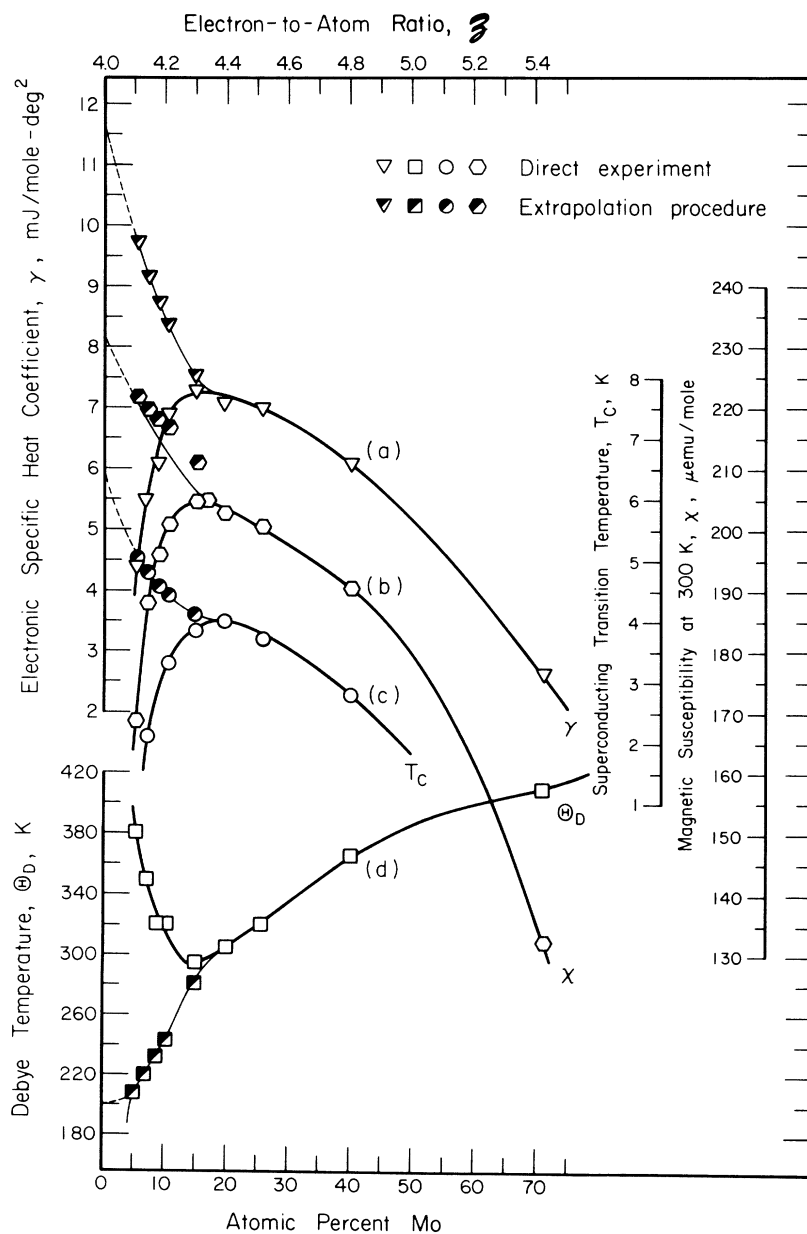


FIG. 5. Calorimetrically derived electronic-specific-heat coefficient γ ; Debye and superconducting transition temperatures Θ_D and T_c , respectively; and total magnetic susceptibility χ for Ti-Mo alloys. χ has been extrapolated as the indirect result of high-temperature experiments, and γ follows suit according to the analysis outlined in Table III. The temperatures T_c and Θ_D , derived from the quotients T_c/Θ_D (Table IV), have been selected as a result of self-consistent extrapolations carried out so as to preserve smoothness, and continuity of T_c , whose directly measured values scale with the directly measured values of both χ and γ .

additional support for the validities of the estimated Θ_D 's for virtual β -Ti-Mo, near the lower limit of the range, is given by the fact that, for compositions close to the critical threshold, two completely different procedures yielded almost similar values of Θ_D namely, 205 ± 5 K (Ti-Mo) and 206 ± 2 K (Ti-Cr) at $\bar{\delta} = 4.1$.

G. Conclusions

Because of the assumptions involved, the foregoing analysis is offered not as a quantitative calculation of either T_c or Θ_D , but rather as a demonstration of self-consistency among the directly measured and/or derived calorimetric, magnetic, and structure properties of low-concentration Ti-Mo alloys leading to the following conclusions.

(i) A derived set of values of T_c/Θ_D for unstable Ti-Mo can be separated into (a) a T_c , which increases monotonically with decreasing $\bar{\delta}$ and (b) a Θ_D which continuously decreases so as to form a low-lying branch as $\bar{\delta}$ enters the unstable regime.

(ii) The T_c so obtained scales with the extrapolated γ (and also of course with the extrapolated χ_{spin} , or χ , from which that quantity was derived). This behavior is consistent with the mutual scaling of the three directly measured quantities T_c , γ , and χ in the quenched alloys.

(iii) The lower set of values assumed by Θ_D in the virtual β -Ti-Mo regime expresses the instability of that lattice. This softening is a precursor to martensitic transformation, which takes place near the composition for which $c_{11} = c_{12}$, and which is accompanied by $\Theta_D = 0$.

(iv) Were it not for microstructural effects which occur as a result of bcc-phase instability below $\bar{\delta} \approx 4.4$ in Ti-Mo, T_c would increase monotonically as $\bar{\delta}$ decreased from 6 to 4.

IV. DISCUSSION

A. Superconductivity in T_1 - T_2 Alloys

Based on the preceding observations we offer

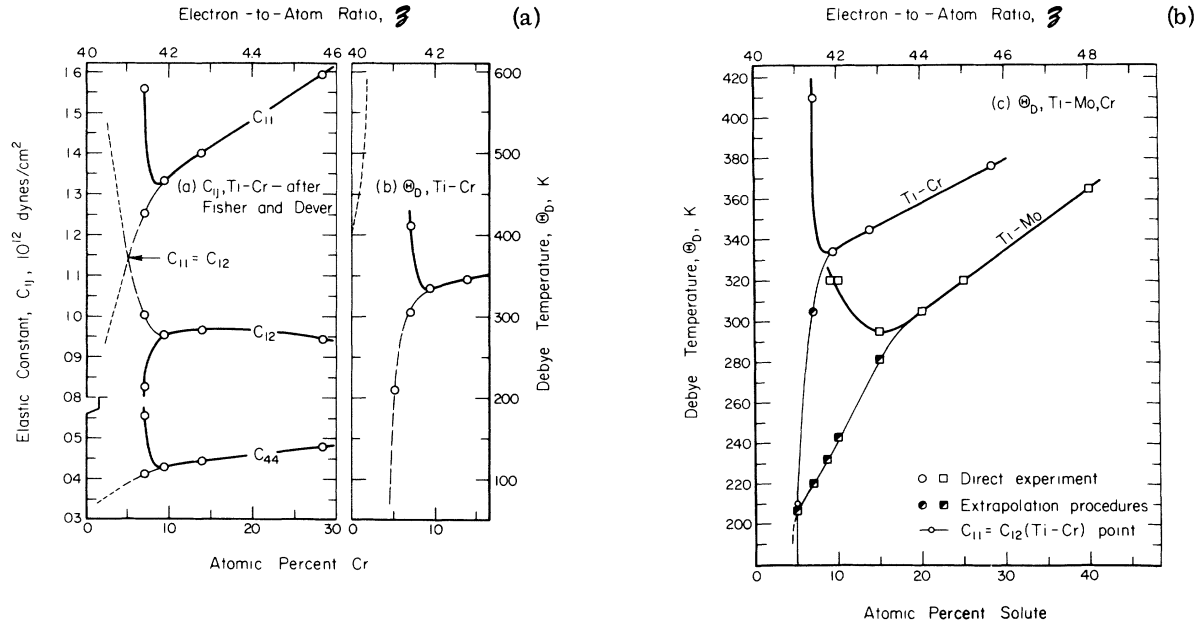


FIG. 6. (a) Elastic constants of Ti-Cr from the tabulated data of Fisher and Dever (Ref. 18). The curves through the extrapolated points have been smoothly extrapolated to 5-at.% Cr (dashed lines), and then linearly extrapolated (chain lines) in order to obtain a set of equations (Appendix B) for use in the calculation of Θ_D in the dilute Ti-Cr regime. (b) Detail showing the behavior of calculated Θ_D [Anderson's method (Ref. 19)] in the critical regimes of ω -phase precipitation, and finally martensitic transformation in anticipation of which Θ_D drops toward zero (dashed curve). The calculated Θ_D is, of course, unphysical in the "absolutely unstable" regime wherein $c_{11} \ll c_{12}$, as indicated by the gap (complex values of Θ_D) $4.05 < \bar{\delta} \leq 4.09$, and the chain line for $4.0 \leq \bar{\delta} \leq 4.05$. (c) Debye temperatures Θ_D for Ti-Mo and Ti-Cr. The value for Ti-Mo was obtained, as a result of the present experiments, either directly or by means of the extrapolation procedures (Tables III and IV). Θ_D for Ti-Cr was calculated from the elastic constants (Refs. 18 and 19); the half-shaded point derived from elastic constants extrapolated by Fisher and Dever (Ref. 18) from the high-temperature equilibrium β field. It is interesting to note that ice-point martensitic transformation occurs in both systems at $\bar{\delta}$ values very close to 4.1, and is preceded by Θ_D values of about 205 K. Differences in the shapes of the curves may be attributed to differences in microstructural character as discussed in Appendix C; in particular, for Ti-Mo, the $(\beta + \omega)$ field seems to be more extensive.

some general comments on the superconductivity of bcc T_1 - T_2 alloys. In Fig. 7, curve a from Ref. 4 shows the behavior of T_c for the $4d$ - $4d$ series. This, along with similarly shaped double-humped curves for the $3d$ - $3d$ and $5d$ - $5d$ sequences exemplifies the Matthias rule as it applies to the T_c 's of T_1 - T_2 alloys in the \bar{z} range 4-8. But, as pointed out in detail above for Ti-Mo and Ti-Cr, and as indicated by the diagram in Fig. 7, the structures assumed by such alloys also depend strongly on \bar{z} . The behavior of T_c in that figure may therefore be correlated (through \bar{z}) with phase stability. T_c is low in the middle of the bcc field where a high stability may be attributed to the half-filled d band. It then increases both with decreasing as well as increasing \bar{z} , attaining maximal values at the limits of bcc stability. Beyond these limits, T_c drops as the structure changes to hcp. The Fermi density of states for T_1 - T_2 alloys is represented by curve b in Fig. 7. The low- \bar{z} segment was constructed from the $n(E_F)$ data for Ti-Mo as listed in Table V, while the remaining portion is a result of the calculations by Snow and Waber²⁰ of $n(E_F)$ for bcc Cr, Mn, and Fe. The manner in which T_c scales

with $n(E_F)$ -related quantities (Fig. 5) and with $n(E_F)$ itself (Fig. 7), and the fact that T_c for bcc Ti-Mo increases monotonically as \bar{z} decreases suggests that, if Ti-Mo-type behavior is typical, T_c vs \bar{z} ($4 < \bar{z} < 8$) would be generally U shaped if the effects of structural changes did not intervene.

Clearly the projected "high" T_c 's at either end of the range under consideration are unattainable since the bcc lattice is unstable there (e.g., $c_{11}-c_{12} < 0$ for $\bar{z} \gtrsim 4.1$ in Ti-Cr). A closer connection between high T_c and lattice instability in T_1 - T_2 alloys can be made by taking one more step with the aid of some of the approximate expressions from Table I. Referring to Eq. (1), if V , the pairing potential, did not change very much we would expect T_c to follow $n(E_F)$, and this is certainly the case. But it is possible to demonstrate by calling on the experimentally observed behavior of V , that T_c (bcc Ti-Mo) increases with decreasing \bar{z} more rapidly than might otherwise have been anticipated. Writing V in the form $V = V_{app}/[1 - n(E_F)V_{app}]$ [Table I, Eqs. (4) and (6)], since experiment has demonstrated that $V_{app} = \text{const}$ for the system under investigation, it follows that V itself increases as $n(E_F)$ increases.

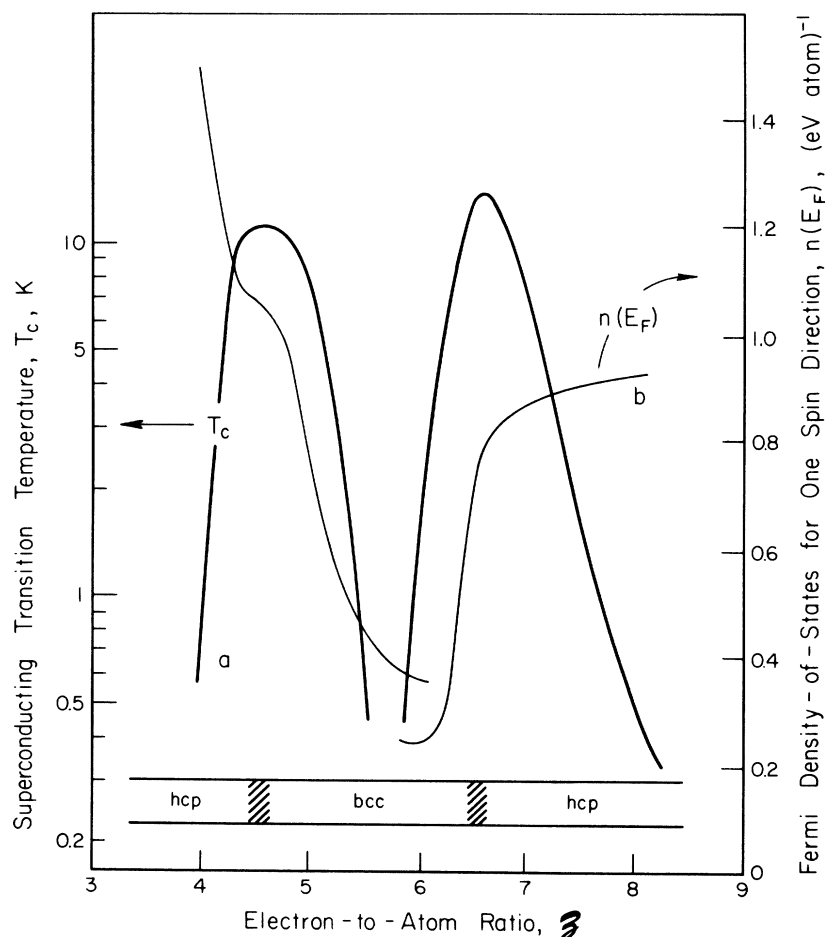


FIG. 7. Curve a from Ref. 4 represents T_c for a sequence of $4d$ - $4d$ T_1 - T_2 alloys. The curves for $3d$ - $3d$ and $5d$ - $5d$ T_1 - T_2 alloys are somewhat similar in shape, the peaks occurring near \bar{z} values of $4\frac{1}{2}$ and $6\frac{1}{2}$, respectively, corresponding to the lower and upper limits of bcc stability. The left-hand segment of curve b connects the $n(E_F)$ data points for Ti-Mo as listed in Table V. The right-hand segment of that curve represents $n(E_F)$ for bcc $3d$ T_1 - T_2 alloys ($6 \leq \bar{z} \leq 8$) as presented by Snow and Waber (Ref. 20), and is based on their calculations of $n(E_F)$ for bcc forms of the pure $3d$ elements Cr, Mn, and Fe. The diagram carries with it the implication that, were it not for structural transformation, the T_c curve for bcc T_1 - T_2 alloys would tend to be U-shaped.

This is shown in Fig. 8 based on the data of Table V. Hence, as the lower limit of bcc stability is approached, T_c , which scales with $n(E_F)V$, increases by virtue of joint increases in both $n(E_F)$ and V . The electron-lattice interaction is, of course, expressed through V which becomes stronger as the density of long-wavelength phonons increases, i. e., as Θ_D decreases. This process is assisted by the approach of lattice instability.

B. Superconductivity in Alloys and Intermetallic Compounds

An intriguing experimental fact recognized by Matthias^{3,4} is that not only do the superconducting transition temperatures of the three sets of T_1 - T_2 alloys ($3d-3d$, $4d-4d$, and $5d-5d$) lie on characteristic double-humped curves, but that a similarly shaped curve is also the envelope of the T_c vs δ points for a multitude of intermetallic compounds.^{3,21} In spite of the present lack of a sophisticated theoretical interpretation of the rule, evidence as strong as this must eventually play a role in some final theory. Equally significant in its own right, but also lacking in rigorous interpretation, is the Engel-Brewer theory²² which relates phase stability of metals and alloys to the spectroscopic states of the participating atoms. Nevertheless, this theory, or set of rules, has had remarkable success in justifying the compositional ranges of various intermetallic structures and alloy systems. In particular, for some classes of alloys and intermetallic compounds it has been possible to make a reasonably significant correlation between the regime of stability of the bcc phase and the existence of a δ within the range 4.4-6.5. Thus, by combining the Matthias and Engel-Brewer rules we have an empirical relationship between superconducting transition temperature and phase stability, with δ as a parameter.

To be more specific we find an interesting, and possibly significant, parallelism between T_1 - T_2 alloys and intermetallic compounds with respect to T_c , lattice stability, and δ . Thus, relatively high T_c 's in both classes of materials are accompanied by a tendency to instability as reflected in the shear modulus $\frac{1}{2}(c_{11} - c_{12})$. We have already pointed this out for Ti-base solid solutions. For the β -W intermetallic compounds, the relationship between high T_c and lattice stability, again as gauged by the behavior of the shear modulus, has been discussed by the Bell Lab group.¹ Based on band-structure calculations, members of the Orsay group² have on one hand discussed the superconducting transition temperatures of β -W compounds, and on the other hand, the elastic moduli. Thus, they too have connected superconductivity to lattice instability, with a special band-structure model based on linear atomic chains as a sufficient but,

TABLE V. Low-temperature superconductive properties of single-phase bcc Ti-Mo alloys, both unstable (0-15-at. % Mo)^a and stable (20-100-at. % Mo).

Alloy Designation Structural Stability of Single-Phase Alloys	Pure Ti														Pure Mo	Comments
	TM-1	TM-2	TM-3	TM-5	TM-7	TM-9-1/2	TM-10	TM-15	TM-20	TM-25	TM-40	TM-70	TM-100			
	Stable at Room Temperature															
γ (mJ/mole-deg ²)	11.5 ₀	11.1 ₅	10.8 ₀	10.4 ₅	9.7 ₆	9.1 ₈	8.7 ₄	8.4 ₀	7.5 ₆	7.1	7.0	6.1	2.6 ₅	1.8 ₅	From Row 14 and part of Row 4, Table 3	
$10^2\lambda$ (number)	63.9	61.4	59.5	57.6	53.8	50.6	48.2	46.3	41.7	39.1	38.6	33.6	14.6	10.2	$\lambda = 0.212 V_{app} \gamma = 0.0551 \gamma$	
χ_{spin} (μ emu/mole)	97.0	94.7	92.8	90.9	87.0	83.6	80.9	76.7	73.2	69.9	62.7	62.7	31.7	23.0	From Rows 8 and 12, Table 3	
T_c (K)	(6.4)				5.05	4.80	4.59	4.42	4.10	4.0	3.7	2.8	<1.5		From Row 5, Table 3; and Table 4	
$n(E_F)$ [(states/eV-atom)]	(1.50)	1.46	1.44	1.41	1.35	1.30	1.25	1.22	1.13	1.08	1.07	0.97	0.49	0.36	$n(E_F) \approx \chi_{spin}/64.7$	
10^2V (eV-atom)	42.6	41.8	41.3	40.9	39.9	38.9	38.6	38.0	36.9	36.2	36.1	34.6	29.8	28.3	$V \approx \lambda/n(E_F)$ - a weak-coupling approximation ^b	

^aData extrapolated into the " α " range $0 \leq [Mo] < 4.5$ at. % must be interpreted with considerable caution.

^bSee, for example, W. L. McMillan, Phys. Rev. **167**, 331 (1968).

presumably, not necessary electronic condition. In the realm of *unstable* materials, we have predicted relatively high T_c 's for virtual bcc Ti-Mo alloys; and Matthias has predicted high T_c 's for β -W forms of Nb_3In , Nb_3Zn , and Zr_3Sb^3 all of which have defied attempts at their preparation presumably because of stability considerations.

V. CONCLUSIONS

A common feature shared by many "high"- T_c intermetallic compounds is their being on the threshold of transforming to structures of lower symmetry. Likewise, in the alloy system Ti-Mo, the

highest T_c occurs just before further decrease in δ introduces a mixed-phase regime. Accordingly, it is suggested that were it not for the intervention of structural transformations, the T_c vs δ (4-8) curves for bcc T_1 - T_1 alloys would be approximately U shaped. The well-known Matthias and Engel-Brewer rules connect T_c and phase stability, respectively, with atomic spectroscopic states, a property which may occasionally be further simplified to δ . In this way we can recognize δ as a link between phase stability and T_c , which provides us with a clue towards understanding the otherwise surprising similarities between the δ dependences

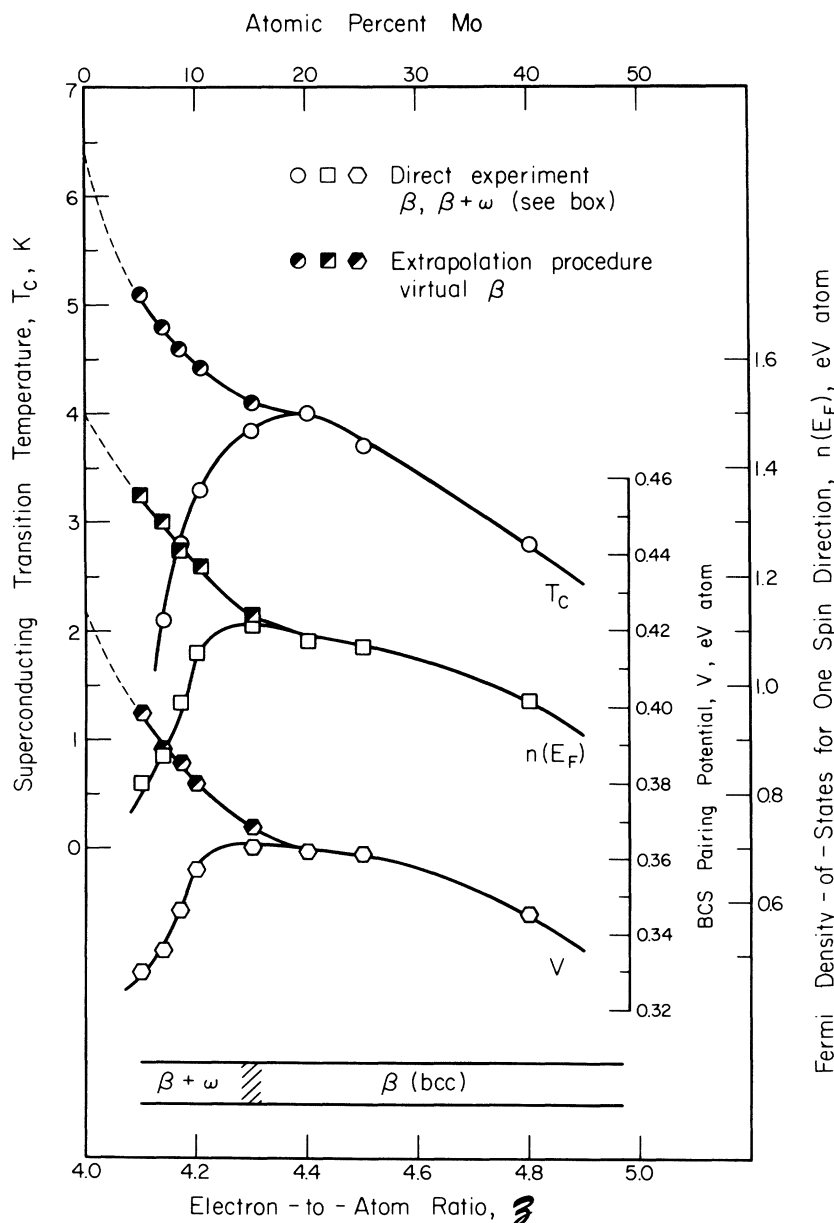


FIG. 8. Superconducting transition temperature T_c , plotted together with the calculated Fermi density of states $n(E_F)$, and pairing potential V , derived according to Table V. The figure demonstrates that, in the BCS-Morel expression $T_c/\Theta_D \propto e^{-1/n(E_F)V}$, T_c increases with decreasing δ , through joint increases in both $n(E_F)$ and V , suggesting that the increase in T_c at low δ values is not simply a density-of-states effect.

of T_c in intermetallic compounds and T_1 - T_2 alloys.

ACKNOWLEDGMENTS

We wish to acknowledge R. D. Smith for technical assistance, and also Dr. L. R. Testardi, Bell Telephone Laboratories, for encouraging and helpful correspondence.

APPENDIX A: DEBYE TEMPERATURES OF Ti-Cr ALLOYS FROM MEASURED ELASTIC CONSTANTS

A standard expression for the Debye temperature Θ_D written in a form applicable to alloys is

$$\Theta_D = \frac{h}{k} \left(\frac{3N}{4\pi} \right)^{1/3} \left(\frac{\rho}{M} \right)^{1/3} v(c_{ij})_m.$$

This yields a value for Θ_D in K, when the various quantities are expressed in cgs units. The product of the first two factors involving atomic constants is 25.1460×10^{-4} deg sec (atom/mole) $^{1/3}$. ρ is the density (g/cm 3), M is the average atomic weight of alloy, and v_m is a function of the elastic constants, c_{ij} , expressed in the units 10^{12} dyn/cm 2 .

For an isotropic material, such as a polycrystalline alloy, v_m may be expressed as a function of some average shear and longitudinal sound velocities. Thus, according to the literature,

$$v_m = \frac{1}{3} \left(\frac{2}{v_s^3} + \frac{1}{v_l^3} \right)^{-1/3}.$$

Anderson¹⁹ has shown that values of Θ_D for various substances, including polycrystalline alloys, may be calculated (Table VI) in an accurate and straightforward manner through the use of the fol-

lowing expressions (using Anderson's symbolism) for v_s and v_l :

$$v_s^2 = G_H/\rho, \quad v_l^2 = (K_H + \frac{4}{3} G_H)/\rho.$$

For substances of cubic symmetry $K_H = \frac{1}{3}(c_{11} + 2c_{12})$, and $G_H = \frac{1}{2}(G_R + G_V)$, in which $G_V = \frac{1}{5}(c_{11} - c_{12} + 3c_{44})$ and $1/G_R = \frac{1}{5}[4/(c_{11} - c_{12}) + 3/c_{44}]$.

APPENDIX B: DEBYE TEMPERATURE OF DILUTE Ti-Cr ALLOYS FROM EXTRAPOLATIONS OF THE MEASURED ELASTIC CONSTANTS

In order to obtain a semiquantitative estimate of the possible behavior of Θ_D as the solute concentration decreases towards the low-concentration boundary ($\alpha'/\beta + \omega$) of the $\beta + \omega$ field, linear extrapolations of Fisher and Dever's¹⁸ elastic constant data [the dashed lines in Fig. 6(a)] were inserted in Anderson's¹⁹ formula. These linearly extrapolated c_{ij} 's were described by

$$\left. \begin{aligned} 10^{-12}c_{11} &= 0.765 + 0.073_5 t \\ 10^{-12}c_{12} &= 1.824 - 0.137 t \\ 10^{-12}c_{44} &= 0.320 + 0.013_2 t \end{aligned} \right\} t \equiv \text{at. \% Cr},$$

and from Fisher and Dever's¹⁸ measured densities for Ti-Cr, and a literature value²³ ($\rho = 4.507$ g/cm 3) for pure Ti,

$$\rho = 4.507 + 0.023_7 t.$$

With this input Θ_D was computed within the range $0 \leq (\text{at. \% Cr}) \leq 9.9$ at intervals of 0.1 at. %. The results, some of which are listed in Table VII, are shown in Fig. 6(b). Of particular interest is the

TABLE VI. Calculation of Θ_D from tabulated elastic constants of Ti-Cr^a using Anderson's method.^b

At. % Cr	6.98	6.98	9.36	13.81	28.37
Metallurgical state	β^c	Brine quenched ^d	Brine quenched ^e	Brine quenched ^f	Brine quenched ^f
Density ρ (g/cm 3)	4.677	4.677	4.725	4.834	5.027
Average molar weight M	48.19	48.19	48.29	48.47	49.07
Elastic constant, $10^{-12}c_{11}$ (dyn/cm 2)	1.250	1.559	1.331	1.399	1.591
$10^{-12}c_{44}$	0.410	0.554	0.427	0.442	0.477
$10^{-12}c_{12}$	1.002	0.825	0.951	0.963	0.941
Average velocity $10^{-4}v_m$ (cm/sec)	26.38	35.44	28.81	29.56	32.03
Θ_D (K)	304.8	409.5	333.8	344.7	376.8

^aReference 18.

^bReference 19.

^cExtrapolated to room temperature from the elevated-temperature β field.

^dRegarded by Fisher *et al.* (Ref. 18) as containing a

substantial fraction of ω phase.

^eEstimated by Fisher *et al.* (Ref. 18) to contain a possible trace of ω phase.

^fSingle-phase bcc (β).

TABLE VII. Some data from the computation of Θ_D for unstable bcc Ti-Cr alloys at 0.1 at. % intervals within the concentration range 0–9.9-at. % Cr.

At. % Cr.	$10^{-12} c_{11}$ (dyn/cm ²)	$10^{-12} c_{12}$ (dyn/cm ²)	$10^{-12} c_{44}$ (dyn/cm ²)	Θ_D (K)
0, 0	0, 765	1, 824	0, 320	401, 0
0, 1	0, 772	1, 810	0, 321	406, 2
0, 2	0, 780	1, 800	0, 323	411, 6
2, 5	0, 949	1, 482	0, 353	928, 7
2, 6	0, 956	1, 468	0, 354	1132, 7
2, 7	0, 963	1, 454	0, 356	1688, 9
2, 8–4, 4				Θ_D , complex
4, 5	1, 096	1, 208	0, 379	69, 9
4, 6	1, 103	1, 194	0, 381	116, 5
4, 7	1, 110	1, 180	0, 382	146, 5
4, 9	1, 125	1, 153	0, 385	187, 8
5, 0	1, 133	1, 139	0, 386	203, 4
(5, 03	1, 135	$c_{12} = c_{11}$	0, 386 ₁	208) ^a
5, 1	1, 140	1, 125	0, 387	216, 9
5, 2	1, 147	1, 112	0, 389	228, 8

^aThe $c_{11} = c_{12}$ crossover point.

sudden decrease exhibited by Θ_D in the composition range $4.5 \leq (\text{at. \% Cr}) \leq 5.5$, centered about the c_{11} , c_{12} crossover point.

APPENDIX C: DISCUSSION OF QUENCHED MICROSTRUCTURES AND bcc-PHASE INSTABILITY IN Ti-Mo AND Ti-Cr ALLOYS

A. Martensitic Transformation

As was pointed out in an earlier publication,¹⁰ rapidly quenched Ti-Mo alloys possessed a dense martensite (α') structure, whereas those studied in the as-cast condition were found to contain only patches of α' . Accordingly, we concluded that in Ti-Mo the transition between the α' and the ($\beta + \omega$) regions occurred at about $4\frac{1}{2}$ -at. % Mo. This observation is included in Figs. 1(b) and 1(c).

From the results of optical metallographic studies on quenched Ti-Cr alloys, Duwez and Taylor²⁴ concluded that the martensitic regime for that system terminated at a concentration between 5.0- and 6.0-at. % Cr. Comparing these data with the results of the elastic-constant studies of Ti-Cr by Fisher and Dever,¹⁸ as presented in Figs. 6(a) and 6(b) and referred to in Appendix B, we deduce that the onset of martensitic transformation in that system is associated with the vanishing of the shear modulus $\frac{1}{2}(c_{11} - c_{12})$ which occurs at 5.0₃-at. % Cr (Table VII).

Combining this conclusion with our observation of the critical (M_s) composition for Ti-Mo, we suggest that it would be consistent to predict a rapid decrease of Θ_D occurring in the Ti-Mo system at about $4\frac{1}{2}$ -at. % Mo. Such a drop is indicated in Fig. 6(c). As a continuation of this program we intend to study the elastic constants of Ti-Mo; however, in the meantime we suggest, by analogy

with the results for Ti-Cr, that an attempt to calculate Θ_D for bcc Ti-Mo could be expected to lead to unphysical results in the Mo concentration range below $4-4\frac{1}{2}$ -at. %, i. e., in "absolutely unstable" Ti-Mo.

B. Precipitation of ω Phase

In general, ω -phase forms from the bcc matrices of quenched Ti- T_2 alloys in a composition range within 10 at. %, more or less, of the martensitic regime. The degree of spontaneity of its occurrence has been discussed by various authors; but at sufficiently high solute concentrations ω phase will form only as a result of diffusion during moderate-temperature aging.²⁵ Electron-diffraction studies of specimens taken from the brine-quenched ingots (~30 g) of Ti-Mo used for the low-temperature specific-heat measurements showed the presence of dense ω -phase precipitation in alloys of compositions 5- and 10-at. % Mo. The photographic evidence has been presented elsewhere.⁷ On the other hand, Hickman,²⁶ using single-crystal x-ray techniques, failed to detect ω phase in rapidly gas-quenched strips of Ti-Mo (8.0, 10.0, and 14.0 at. %). However, ω phase was seen to develop in the first two of these alloys during aging. The disagreement between Hickman's observations and our own is significant, and emphasizes the importance of quench rate as a factor governing the observability of ω phase in quenched Ti- T_2 alloys in general. An x-ray diffraction study in this laboratory of quenched single-crystalline TM-20,²⁷ although failing to reveal the presence of any ω phase, showed evidence of clustering, a phenomenon not unexpected in a nonequilibrium alloy quenched to within its ($\alpha + \beta$) phase field [c. f. Figs. 1(a) and 1(b)]. Although a direct search for ω phase was not carried out on TM-15 the behaviors of the electronic properties themselves suggest that, even if a (microscopically) observable precipitate is not present, metallurgical effects at least precursive of it (such as clustering) are present.

Similarly, in the case of quenched Ti-Cr, Fisher and Dever,¹⁸ using the indirect evidence of their elastic constant work, have suggested that a substantial fraction of ω phase was present in Ti-Cr (6.98 at. %), while a slight amount may have been present in the quenched 10.08-at. % alloy. That conclusion was substantiated by the observations of Hickman,²⁶ who claimed to have detected ω phase in quenched Ti-Cr (9.3 at. %). On the other hand, Erickson *et al.*,²⁸ in a study of the alloy series Ti-Cr (5.5, 5.9, 6.4, 7.6, 8.0, 11.3, and 18.7 at. %), failed to find ω phase in alloys above 8-at. % Cr. In view of the sensitivity of " $\beta + \omega$ " alloys to slight differences in aging and heat treatment it is always preferable to carry out microstructural studies, if they are to be made, on the actual spec-

imens whose physical properties are being measured. Such direct evidence was not available for the Ti-Cr elastic-constant specimens; however, the above-mentioned metallurgical observations certainly serve to substantiate Fisher and Dever's estimate of the microstructural states of their alloys (Table VI).

Taking all the relevant metallurgical and physical property evidence into consideration it is possible to compare the composition dependences of the Debye temperatures of Ti-rich Ti-Mo and Ti-Cr [Fig. 6(c)] in the following way.

In Ti-Mo, incipient or real ω phase precipitation commences at about 15-at.% Mo ($\delta \approx 4.3$) and increases in density, as [Mo] decreases, resulting

in a pronounced stiffening of the lattice. The corresponding instability of the virtual bcc lattice in this concentration range is reflected in the behavior of the extrapolated Θ_D which decreases to form a lower lying branch for TM-15 and below. At TM-4 $\frac{1}{2}$, the martensitic transformation point, we predict a rapid drop in Θ_D . In Ti-Cr the experimental evidence suggests that bcc phase instability becomes appreciable at a lower solute concentration than is the case for Ti-Mo alloys. This brings the composition at which Θ_D starts to turn downwards [Fig. 6(c)] fairly close to the martensitic transformation point itself. As a result, Θ_D for Ti-Cr decreases much more steeply to zero than does that for Ti-Mo.

*Work supported by Battelle, Columbus Laboratories, and the Air Force Materials Laboratory, Wright-Patterson Air Force Base.

[†]Present address: Physics Dept., Wichita State University, Wichita, Kan. 67208.

¹L. R. Testardi, T. B. Bateman, W. A. Reed, and V. G. Chirba, *Phys. Rev. Letters* **15**, 250 (1965); L. R. Testardi, *Phys. Rev. B* **3**, 95 (1971); L. R. Testardi, J. E. Kunzler, H. J. Levinstein, J. P. Maita, and J. H. Wernick, *ibid.* **3**, 107 (1971); J. C. Phillips, *Phys. Rev. Letters* **26**, 543 (1971).

²J. Labbé, S. Barišić, and J. Friedel, *Phys. Rev. Letters* **19**, 1039 (1967); J. Labbé, *Phys. Rev.* **172**, 451 (1968).

³B. T. Matthias, in *Superconductors*, edited by M. Tanenbaum and W. V. Wright (Interscience, New York 1962), p. 1.

⁴B. T. Matthias, *Am. Scientist* **58**, 80 (1970).

⁵F. Heiniger, E. Bucher, and J. Muller, *Physik Kondensierten Materie* **5**, 243 (1966).

⁶J. C. Ho and E. W. Collings, *Phys. Letters* **29A**, 206 (1969).

⁷E. W. Collings and J. C. Ho, *Natl. Bur. Std. (U. S.) Spec. Publ. No. 323*, 1971 (unpublished), p. 587. Recent reanalysis has called for some very slight alterations in the numerical data presented in the inset to Fig. 9 in this reference. The updating is carried out in the present paper (Tables III and V, and Fig. 4).

⁸*Electrorefined Ti sponge*, grade ELXX from the Titanium Metals Corp., contained as principal impurities in wt% O, 0.037; N, 0.004; Cl, 0.073; Fe, 0.009. *The Mo*, from Climax Molybdenum Co., contained as principal impurities in wt% C, 0.014; O < 0.0004; H < 0.0001; N < 0.0001; Fe < 0.006; Ni < 0.001; Si < 0.002.

⁹E. W. Collings and J. C. Ho, *Phys. Letters* **29A**, 306 (1969).

¹⁰E. W. Collings and J. C. Ho, *Phys. Rev. B* **1**, 4289 (1970).

¹¹J. C. Ho and E. W. Collings, *J. Appl. Phys.*, **42**,

5144 (1971).

¹²D. W. Budworth, F. E. Hoare, and J. Preston, *Proc. Roy. Soc. (London)* **257**, 250 (1960).

¹³J. Bardeen, L. N. Cooper, and J. R. Schrieffer, *Phys. Rev.* **108**, 1175 (1957).

¹⁴P. Morel, *J. Phys. Chem. Solids* **10**, 277 (1959).

¹⁵In an earlier publication [E. W. Collings and J. C. Ho, *Phys. Letters* **31A**, 193 (1970)] it was assumed that $\chi_{\text{orb}} = \text{const} = 132 \mu\text{emu/mole}$ for [Mo] ≤ 20 at. %.

We now prefer to assign a negative composition dependence to χ_{orb} ([Mo]) over the entire concentration range. As shown in Fig. 4, extrapolation of the "measured" data yields $\chi_{\text{orb}}(\text{Ti}_{\text{bcc}}) = 134 \mu\text{emu/mole}$.

¹⁶E. W. Collings and J. C. Ho (unpublished).

¹⁷A. K. Sinha, *J. Phys. Chem. Solids* **29**, 749 (1968).

¹⁸E. S. Fisher and D. Dever, *Acta Met.* **18**, 265 (1970).

¹⁹O. L. Anderson, *J. Phys. Chem. Solids* **24**, 909 (1963).

²⁰E. C. Snow and J. T. Waber, *Acta Met.* **17**, 623 (1969).

²¹B. W. Roberts, *Natl. Bur. Std. (U. S.) Tech. Note No. 482*, 1969 (unpublished).

²²L. Brewer, in *Phase Stability in Metals and Alloys*, edited by P. S. Rudman, J. Stringer, and R. I. Jaffee (McGraw-Hill, New York, 1967), p. 39.

²³E. K. Molchanova, *Phase Diagrams of Titanium Alloys*, edited by S. G. Glazunov (Israel Program on Scientific Translations, Jerusalem, 1965), p. xvii.

²⁴P. Duwez and J. L. Taylor, *Trans. Am. Soc. Metals* **44**, 495 (1952).

²⁵Yu. A. Bagaryatskii and G. I. Nosova, *Fiz. Metal. Metalloved* **13**, 415 (1962).

²⁶B. S. Hickman, *Trans. AIME* **245**, 1329 (1969).

²⁷P. C. Gehlen, AFML Technical Report No. AFML-TR-70-1, 1969 (unpublished).

²⁸R. H. Ericksen, R. Taggart, and D. H. Polonis, *Trans. AIME* **245**, 359 (1969).